


## RESEARCH ARTICLE

Structural stability and the low-lying singlet and triplet states of BN-*n*-acenes, *n* = 1–7

Bruno D. Milanez<sup>1</sup> | Gustavo M. dos Santos<sup>1</sup> | Max Pinheiro Jr<sup>1</sup> |  
Leonardo T. Ueno<sup>1</sup> | Luiz F. A. Ferrão<sup>1</sup> | Adelia J. A. Aquino<sup>2</sup> | Hans Lischka<sup>3</sup> |  
Francisco B. C. Machado<sup>1</sup> 

<sup>1</sup>Department of Chemistry, Instituto Tecnológico de Aeronáutica (ITA), São Paulo, Brazil

<sup>2</sup>Department of Mechanical Engineering, Texas Tech University, Lubbock, Texas, USA

<sup>3</sup>Department of Chemistry and Biochemistry, Texas Tech University, Lubbock, Texas, USA

## Correspondence

Hans Lischka, Department of Chemistry and Biochemistry, Texas Tech University, Lubbock, Texas 79409, USA.

Email: [hans.lischka@univie.ac.at](mailto:hans.lischka@univie.ac.at)

Francisco B. C. Machado, Department of Chemistry, Instituto Tecnológico de Aeronáutica (ITA), São José dos Campos 12228-900, São Paulo, Brazil.

Email: [fmachado@ita.br](mailto:fmachado@ita.br)

## Funding information

Fundação de Amparo à Pesquisa do Estado de São Paulo, Grant/Award Numbers: 2019/03729-8, 2019/25105-6; Conselho Nacional de Desenvolvimento Científico e Tecnológico, Grant/Award Numbers: 307136/2019-1, 313624/2019-4; National Science Foundation, Grant/Award Number: 2107923

## Abstract

The chemical stability and the low-lying singlet and triplet excited states of BN-*n*-acenes (*n* = 1–7) were studied using single reference and multireference methodologies. From the calculations, descriptors such as the singlet-triplet splitting, the natural orbital (NO) occupations and aromaticity indexes are used to provide structural and energetic analysis. The boron and nitrogen atoms form an isoelectronic pair of two carbon atoms, which was used for the complete substitution of these units in the acene series. The structural analysis confirms the effects originated from the insertion of a uniform pattern of electronegativity difference within the molecular systems. The covalent bonds tend to be strongly polarized which does not happen in the case of a carbon-only framework. This effect leads to a charge transfer between neighbor atoms resulting in a more strengthened structure, keeping the aromaticity roughly constant along the chain. The singlet-triplet splitting also agrees with this stability trend, maintaining a consistent gap value for all molecules. The BN-*n*-acenes molecules possess a ground state with monoconfigurational character indicating their electronic stability. The low-lying singlet excited states have charge transfer character, which proceeds from nitrogen to boron.

## KEYWORDS

acene analogues, borazine, excited states, stability

## 1 | INTRODUCTION

Borazine is a highly interesting compound, which is often called “inorganic benzene” because of its similarity to benzene. However, the electronegativity difference between boron and nitrogen causes the delocalization of  $\pi$  electrons to be reduced in comparison to benzene<sup>1–3</sup> and the existence of boron-nitrogen polar bonds also induces reactivity differences between borazine and benzene.<sup>4,5</sup> Borazine has generated interest as a precursor for obtaining nanotubes<sup>6</sup> and boron nitride ceramics.<sup>7</sup> These ceramics have properties such as high thermal and chemical stability for corrosion and oxidation, among

others.<sup>8</sup> Another important area of research is the use of boron nitride for hydrogen storage in fuel cells.<sup>9,10</sup>

The spectroscopy of borazine has been under discussion for a long time. Platt et al.<sup>11–13</sup> studied the spectrum in the ultraviolet region and found two bands, one starting at 6.21 eV and another, very intense one, with a maximum at 7.20 eV. This last band is related to the  $^1E' \leftarrow ^1A'_1$  transition,<sup>11</sup> while the less intense absorptions at 6.5 and 6.7 eV are related to  $^1A'_2 \leftarrow ^1A'_1$  and  $^1A'_1 \leftarrow ^1A'_1$  transitions, respectively.<sup>13</sup> Kaldor obtained the absorption spectrum for borazine in the vapor phase and isolated it in an argon matrix, detecting the same types of transitions.<sup>14</sup> Several theoretical calculations have been

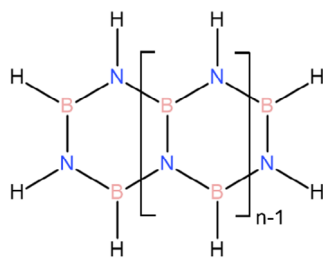


**FIGURE 1** Representation of the BN-*n*-acenes, *n* = 1–7

performed for the characterization of the excited states of borazine. The first one was performed by Roothaan and Mulliken already at the time of the first experimental investigations.<sup>15</sup> A wide range of theoretical approaches have been considered using methods such as the Pariser-Parr-Pople-type self-consistent field (SCF) approach,<sup>16–19</sup> semiempirical self-consistent field-molecular orbitals (SCF-MO),<sup>20</sup> SCF MO and configuration interaction (CI),<sup>21</sup> and time-dependent density functional theory (TDDFT)<sup>22</sup> calculations.

Starting from borazine, the increase in the number of fused BN rings creates one-dimensional (1D) BN-*n*-acene quasi-linear structures, or BN-polyacenes, which are isoelectronic and structurally similar to polyacenes. The polyacenes have  $D_{2h}$  symmetry with the first two lowest singlet excited states of  $B_{2u}$  and  $B_{3u}$  symmetry. The corresponding states for BN-polyacenes have  $B_2$  and  $A_1$  symmetry within the  $C_{2v}$  point group (Figure 1). The character of these states will be affected by the intrinsic dipole moment along the shorter axis due to the asymmetry on the zig-zag edges due to boron and nitrogen alternation.

For the systems larger than borazine, the only few experimental data available have been reported for mass spectrometric detection and x-ray characterization of BN-naphthalene.<sup>23–25</sup> Theoretically, to our knowledge, only a few studies have been carried out on the stability, reactivity and aromaticity of BN-naphthalene,<sup>26–29</sup> one of them describe the UV-vis spectra using the CC2/def2-TZVPPD methodology. In addition, up to BN-pentacene, some calculations have been performed discussing aromaticity.<sup>5,30</sup> In particular, no experimental or theoretical investigations on excited states of the BN-*n*-acenes with *n* > 1 have been performed.

In this work, the chemical stability of BN-*n*-acenes (*n* = 1–7) was studied based on descriptors such as the biradical character or the singlet-triplet (ST) splitting considering different methodologies to obtain a systematic picture of the chain-length dependence of their properties. This analysis is based on high-level quantum chemical approaches ranging from single reference to multireference methods to obtain reliable information about the structure, the energetic stability, and insights about the biradical character, using descriptors such as the singlet-triplet (ST) splitting, the natural orbital (NO) occupations and aromaticity indexes. The ST splitting is fundamental in the stability discussion to access how easily the systems can be excited and reach a more reactive state. An investigation of charge transfer effects within the structures is also performed since they form characteristic features in the borazine series. Based on these results, comparisons

with the acene series can be made to elaborate on the interesting differences between these two paradigmatic classes of compounds.

## 2 | METHODOLOGY

All structures studied were optimized using Møller-Plesset second order perturbation theory (MP2)<sup>31</sup> with the split-valence plus polarization def2-TZVP basis set.<sup>32</sup> Borazine has  $D_{3h}$  symmetry and the other structures  $C_{2v}$ , but all calculations were performed with  $C_{2v}$  symmetry. All molecules investigated are planar and are located within the *yz* plane, with the  $C_2$  axis corresponding to the *z* axis. The equilibrium geometries are available in the Supporting information file, see Tables S1–S7 with the cartesian coordinates of each system.

The structural aromaticity of the molecules was investigated in terms of the harmonic oscillator model of aromaticity (HOMA),<sup>33</sup> which is a geometry-based estimator of aromaticity. This index is calculated for each six-membered cycle of the molecules according to the formula:

$$\text{HOMA} = 1 - \frac{\alpha}{n} \sum (R_{\text{opt}} - R_i)^2, \quad (1)$$

where  $R_{\text{opt}}$  is a reference optimal value for the bond length which leads to HOMA = 1 for benzene, *n* is the number of bonds in the ring, and  $\alpha$  is a normalization factor which guarantees values for HOMA close to 1 for aromatic systems and close to 0 for a non-aromatic structure, the parameters depend on the type of connectivity. The  $R_i$ 's represent the bond lengths of the optimized compounds. Since the B–N bond is quite different from the C–C bond in benzene, as it is strongly polarized resulting in deviations from the covalent character, Madura et al.<sup>34</sup> suggested using, for the B–N connectivity, values of  $\alpha$  and  $R_{\text{opt}}$  equal to 72.03 and 1.402 Å, respectively. For the C–C connectivity, the parameters are  $\alpha = 257.7$  and  $R_{\text{opt}} = 1.388$  Å.<sup>33</sup>

To support the structural discussion, the natural population analysis (NPA) was applied using the MP2 relaxed densities. Contributions of charges in the  $\pi$  and  $\sigma$  domains were obtained separately to analyze the charge transfer within the molecules.

Natural orbital occupations were calculated based on the multireference (MR) averaged quadratic coupled cluster (MR-AQCC)<sup>35</sup> method. For calculations of excited states the complete active space self-consistent field (CASSCF),<sup>36–38</sup> the internally contracted multireference configuration interaction (ic-MRCI),<sup>39–41</sup> with Davidson's correction (ic-MRCI+Q),<sup>42,43</sup> and the complete active-space second-order perturbation theory (CASPT2) were used.

The stability was also analyzed from the radical character of the BN-*n*-acenes by considering the natural orbital (NO) occupations as computed from the MR-AQCC<sup>35</sup> /6-31G\*<sup>44</sup> density by analyzing the deviations of individual NO occupations  $n_i$  from zero (unoccupied) and two (doubly occupied). These single point calculations were carried out using the singlet optimized MP2 geometries with

an active space of eight electrons in eight  $\pi$ -orbitals, CAS (8,8), which was chosen based on the AQCC natural orbitals ranked by their occupation numbers. The MR-AQCC wave functions were constructed allowing all single and double excitations within the total  $\pi$ -space (occupied and virtual) applying the interacting space restriction.<sup>45</sup>

Finally, the chemical stabilities of the BN-*n*-acenes were analyzed using the singlet-triplet gap obtained from the CASSCF multireference calculations of the low-lying excited singlet and triplet states, applying the complete valence  $\pi$  space for borazine and BN-naphthalene and up to CAS (14,14) for the rest of the systems. The multireference calculations were performed using the 6-31G\* basis set, except for borazine, in which the smaller size of the molecule allowed us to also use the def2-TZVP basis set.<sup>32</sup>

The excited states calculations were first carried out with the state-averaged SA-CASSCF<sup>36–38</sup> method to generate the molecular orbitals and the configuration state functions to be used in the next step using multi-state MS-CASPT2<sup>46,47</sup> and internally contracted multireference configuration interaction (ic-MRCI) calculations, the latter being applied only to borazine. A level shift of 0.2 au was used to avoid intruder states in the CASPT2 calculations. Calculations using the full  $\pi$  active reference space were possible only for systems with one to three fused rings. For systems with more than three rings, the use of the full  $\pi$  active space becomes impractical, and therefore, the analysis of the natural orbitals occupation is an important aid for choosing the active space orbitals, which was done primarily from AQCC calculations (see Table S8). The active space was chosen including orbitals with occupation ranging from 0.03 to 1.94 e. We have also performed calculations using excitation restrictions (RAS) for BN-anthracene to calibrate a standard methodology to be adopted in the study of larger systems based on the previous study for *n*-acenes.<sup>48</sup> Thus, several CASSCF and CASPT2 calculations were performed using the CAS active space with the inclusion of occupied and virtual orbitals with excitation restrictions (RAS). To verify the influence of the  $\sigma$  orbitals in the characterization of excited states, the calculations were carried out freezing the sigma orbitals originated essentially from the 1s orbitals (1s), and for the ones originated from the 1s plus 2s orbitals (1s2s).

All MP2 geometry optimizations and NPA calculations were performed using the Gaussian 09 computational code.<sup>49</sup> The ic-MRCI

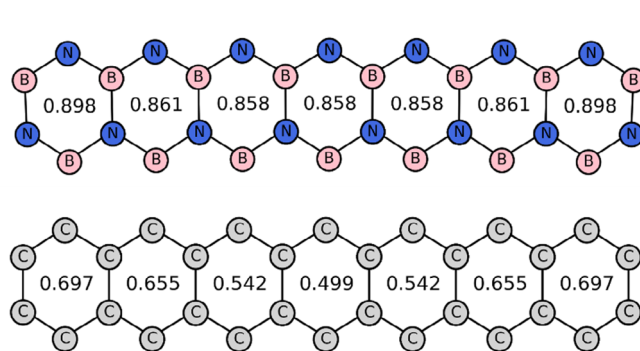
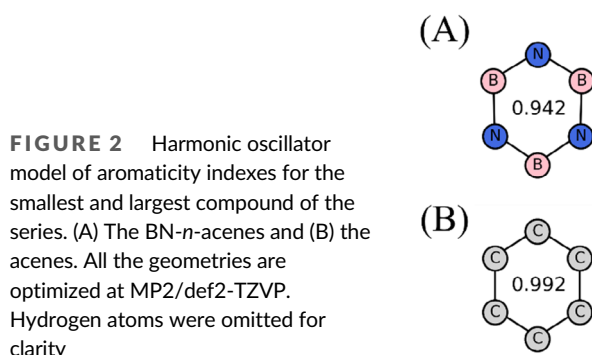
and CASPT2 calculations were performed using the MOLPRO software<sup>50</sup> and the MR-AQCC calculations were carried out using the parallel version of the COLUMBUS program system.<sup>51,52</sup>

### 3 | RESULTS AND DISCUSSION

#### 3.1 | Structure of the BN-*n*-acenes

Based on the optimized geometries, HOMA values provide a compact evaluation of the aromaticity of the BN-*n*-acenes in comparison to the corresponding acenes.<sup>53</sup> It should be noted that HOMA values can be used only for internal comparison within either the acene or the BN-*n*-acene series because of different parametrization of the two compound types. Thus, the HOMA values of the acenes can only be compared to that of benzene whereas the HOMA values of the BN-*n*-acenes have borazine as reference. Figure 2A illustrates the calculated HOMA indices for each ring in borazine and BN-heptacene (Figure S1 of the SI shows the results for all the other systems). For comparison, Figure 2B displays the HOMA values for the benzene and heptacene. For the acene series the HOMA decreases significantly as the system becomes larger and also decreases when going from the external to the innermost rings.<sup>54–57</sup> As expected, the present results agree with previous one based on DFT optimized geometries.<sup>56</sup> For example, in heptacene the HOMA values vary from 0.69 to 0.49, leaving the outermost rings with higher aromaticity, similar results were found for the octacene.<sup>58,59</sup>

The HOMA value in BN-naphthalene (0.900) is smaller than in borazine (0.942) by 0.042, which is much smaller than the difference from benzene to naphthalene, equaling to 0.16. As the BN-*n*-acene system continues to increase up to seven fused rings, the HOMA index decreases only slightly from BN-naphthalene to BN-heptacene, the outer ring has always the largest value (0.89) and the inner rings have a value of  $\sim 0.86$  (Figures 2A and S1). The HOMA values indicate that the aromaticity remains practically constant in the BN-*n*-acene series signifying a maintenance of high stability, possibly due to the charge transfer that allows the  $\pi$  electrons in all rings to have similar  $\pi$ -delocalization, but with central rings being slightly less aromatic. The behavior of an almost constant aromaticity for this kind of systems was also reported in terms of Nucleus-Independent Chemical Shifts (NICS).<sup>5,30</sup>



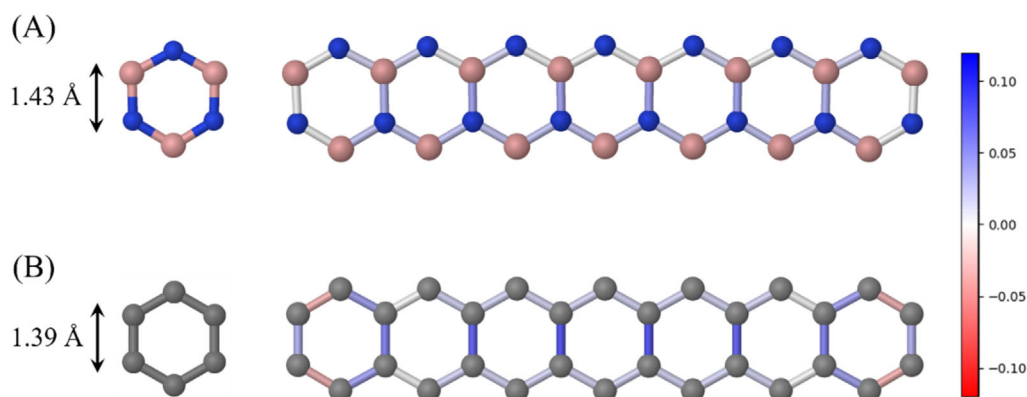


**FIGURE 3** Visualization of the color-coded bond deformations with the increase of the systems, the scale indicates the difference between the calculated bond length and the reference of the smallest compound of the series. (A) The behavior of the BN-*n*-acenes with the bond length reference of 1.43 Å (of the borazine) and (B) the behavior of the acenes with the bond length reference of 1.39 Å (of the benzene). Scale is in Å and hydrogen atoms were omitted for clarity

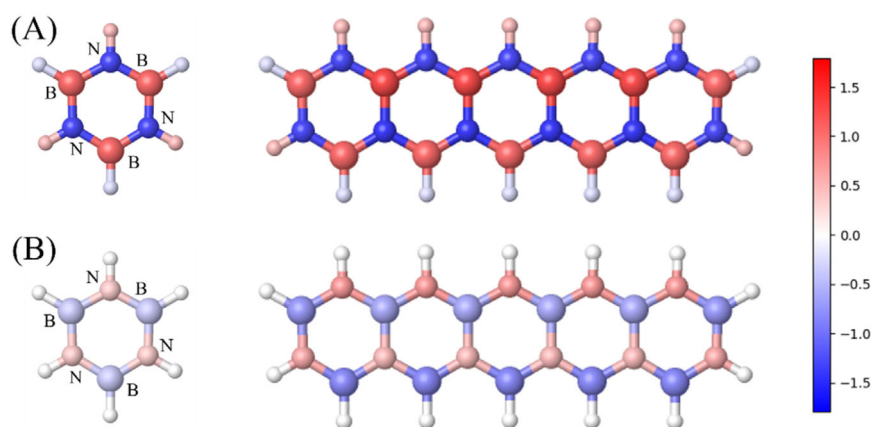


**FIGURE 4** Visualization of the color-coded natural population analysis (NPA) charges (e) for borazine and BN-pentacene. (A) The total NPA net charge and (B) the net  $\pi$  charge. Within the hexagonal rings, boron atoms are represented by the larger spheres and nitrogen atoms by the smaller ones

The alternation of the boron and nitrogen atoms uniformly polarizes the bonds and there are no substantial deformations in the structure with the addition of more rings. It is interesting to quantify the degree of these deformations in the system, Figure 3 shows a colormap characterization of each bond, bluish color indicates an extension, and a reddish color indicates a contraction when compared to the reference of the benzene and borazine. The BN framework (Figure 3A) does not display large variations, the bonds display slight extensions in the ring bonds, the maximum difference is around 0.027 Å. The acene framework (Figure 3B) exhibits a more intense deformation with significant extensions in the ring bonds leading to a greater deviation from the benzene reference. The smaller degree of deformations with the increase of the BN-*n*-acene framework relates to the conservation of high values of HOMA relative to borazine.

In conclusion, for BN-*n*-acenes, the HOMA index and bond deformations show that aromaticity is almost constant, while in the acenes the aromaticity undergoes reduction as the system grows. This does not imply a direct comparison between the aromaticity of the two series since they refer to different reference units (borazine and benzene). A mixing of CC and BN pairs has been investigated

recently<sup>60</sup> where a significantly larger variation of electronic properties had been observed.

### 3.2 | Charge distribution

The structural stability can also be analyzed by means of the interconnectivity of atoms. In general, covalent bonds maintain the interaction across the structure, but as indicated before, the uniform distribution of alternate boron and nitrogen atoms implies a polarization in the backbone bonds of the BN-*n*-acene, which is the result of the simultaneous presence of electrons and holes along the molecule. The resulting local charge transfer is quantitatively described in terms of the NPA charge. Figure 4 presents a color map illustration of the total net charge, Figure 4A, and of the net  $\pi$  charge in Figure 4B, for borazine and BN-pentacene (numerical values are presented in Table S9 for all systems). Overall, the charge distributions show the same pattern throughout the series. First, is noted that the boron gets density from nitrogen in the  $\pi$  domain because of the empty  $\pi$  orbital in the former atom, but loses electron density in the sigma system because of electronegativity differences, as shown

by the resulting colors in Figure 4A,B. In the total charge, nitrogen possesses a negative net charge but the net  $\pi$  charge is positive as it loses electrons to boron.

The resulting charges are dependent on the connectivity of the atoms. This is the reason that, for example, in the BN-pentacene the boron total net charges range from  $\sim 0.9$  to  $\sim 1.2$  e. The boron atoms that are connected to only two nitrogens have smaller positive total net charges in comparison to the ones connected to three nitrogens, which are more positively charged. There are also smaller effects noted on the atoms positioned in the central or outer rings of the molecule. The same connectivity effects lead to concomitant differences for the nitrogen charges that ranges from  $\sim -1.15$  to  $\sim -1.26$  e, where the smaller modulus values belong to N atoms connected only to two B atoms, and the larger modulus values are assigned to the N atoms connected to three B atoms. For the borazine, as there is only one ring there is only one type of connectivity, which is boron connected to two nitrogens and vice versa resulting in charges around  $-1.15$  e for nitrogen and  $0.88$  e for boron.

The hydrogen atoms possess only charge in the  $\sigma$  system. Therefore, hydrogen atoms are colored only in Figure 4A. The atom to which the hydrogen is connected defines the resulting charge. When connected to nitrogen, it will assume a positive charge and when connected to boron it assumes a negative charge, following the respective electronegativities of the atoms.

Additionally, a complementary analysis of the electrostatic potential was performed. The potential is positive in the region of the hydrogen atoms connected to N, and negative for hydrogens connected to B, which confirms the polarization of the hydrogen charges in the respective positions. The nitrogen connectivity brings a more intense polarization and that agrees with the charge values of the NPA analysis that indicates a net charge almost four times greater (in absolute value) for hydrogen connected to nitrogen (around  $0.39$  e) than for hydrogen connected to boron (around  $-0.11$  e), see Table S9. Figure S2A,B shows the plot of the electrostatic potential<sup>61,62</sup> of borazine and BN-pentacene, respectively.

### 3.3 | Frontier orbitals

For the *n*-acenes, the evolution of a pronounced fractional occupation in the highest occupied natural orbital/lowest unoccupied natural orbital (HONO/LUNO) has been observed with increasing system size with occupations starting to deviate significantly from doubly occupied and unoccupied<sup>63</sup> indicating significant polyradicaloid character. On the contrary, in the case of the BN derivatives, the increase in the system size does not cause any significant changes in the occupation of the frontier natural orbitals. For a given BN-*n*-acene,  $NO_{occ} \approx 2$  for  $NO_{index} \leq 2n + 1$  and  $NO_{occ} \approx 0$  for  $NO_{index} > 2n + 1$ , see Figure S3. No intermediate occupation values are detected, and therefore, unpaired electron configurations are not found as important characteristics in these molecules, which is also a sign of stability of these systems.

Another indicator of the stability of the BN-*n*-acenes is based on the analysis of the multiconfigurational character of the wave function. In the following section about the Excited States, there is a more complete discussion and presentation of results concerning the weight of the multiple configurations in the wave function. However, the high degree of monoconfigurational (closed shell) character in the ground state of the BN-systems can be used as evidence to show the high stability of these systems. Indeed, for the BN-*n*-acenes ground state, the contribution of the Hartree-Fock (HF) closed-shell configuration obtained from the  $\pi$ -MR-AQCC wavefunction is 96, 93, 91, 89, 87, 85, and 83% for the first seven members of the BN-*n*-acenes family starting from borazine.

The strong separation of occupied and unoccupied frontier orbitals as shown in the strong occupation gap of the HONO and LUNO orbitals can also be followed in terms of highest occupied molecular orbital (HOMO) and lowest unoccupied molecular orbital (LUMO) energy gaps. The orbital plots for the larger BN-*n*-acenes (Figures S4–S9), and Figure 5 for BN-pentacene, show the HOMO density more concentrated on the nitrogen atoms while the LUMO density is more located on the boron atoms, which agrees with the fact that the boron inherits an empty orbital from the atomic configuration when compared to carbon and will behave as an electron acceptor. The spatial localization of the frontier orbitals on the

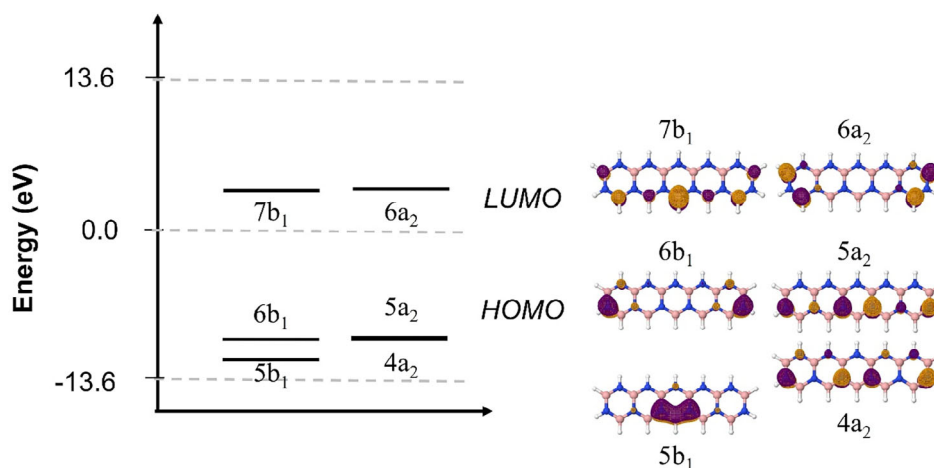


**FIGURE 5** Selected frontier orbitals for the BN-pentacene, with relative energies and respective plots. Results obtained at CASSCF(8,8)/RAS (6,6)/6-31G\* level



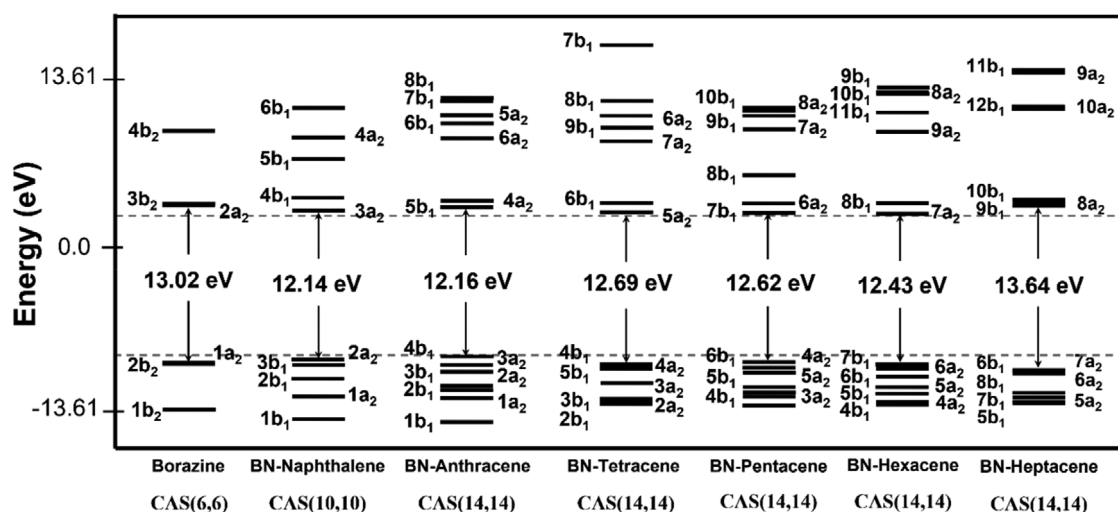


**FIGURE 6** Comparative view of the frontier orbitals for BN-*n*-acenes

**TABLE 1** CASPT2-1s2s/6-31G\* singlet ( $1^1A_1$ )–triplet ( $1^3A_1$ ) splittings  $\Delta E_{1ST}$  and  $\Delta E_{2ST}$  for THE BN-*n*-acenes

BN- <i>n</i> -acenes	$\Delta E_{1ST}$ (eV)	$\Delta E_{2ST}$ (eV)
Borazine	6.74	6.74
BN-naphthalene	6.59	6.59
BN-anthracene	6.62	6.62
BN-tetracene	6.71	6.62
BN-pentacene	6.83	6.64
BN-hexacene	6.78	6.69
BN-heptacene	6.81	6.57

nitrogen and boron atoms (for the occupied and unoccupied orbitals, respectively) reduces the spatial overlap. Therefore, their energy splitting of the orbitals is large (see Figure 6).

The HOMO-LUMO gaps have an average value of 12.7 eV. However, a clear pattern within the series was not found showing a non-monotonic evolution of the energy gap, which oscillates between 12.14 and 13.64 eV (Figure 6). The behavior for the *n*-acenes is the quite different<sup>64,65</sup>: as the size of the system increases the HOMO-LUMO gap reduces significantly. An interesting aspect to be highlighted for the BN-series is the presence of pairs of almost degenerate frontier orbitals. This characteristic is already present in borazine because of the  $D_{3h}$  symmetry but persists also in the larger chains of  $D_{2h}$  symmetry where the degeneracy is not enforced by symmetry.

### 3.4 | Singlet-triplet splitting

The HOMO-LUMO energy gap analysis of the previous section is paralleled by the ST splitting energies. Table 1 shows the calculated values for the first vertical singlet ( $1^1A_1$ ) to triplet ( $1^3A_1$ ) excitation. Defining the selected singlet-triplet splittings,  $\Delta E_{1ST}$ , and  $\Delta E_{2ST}$  were

obtained with CASSCF (8,8)/CASPT2-CAS(8,8)RAS(4,4)-SD and CASSCF (14,14)/CASPT2-CAS(8,8)RAS(6,6)-SD, respectively. In addition, for borazine, BN-naphthalene and BN-anthracene, the complete valence  $\pi$  spaces CAS (6,6), CAS (10,10) and CAS (14,14) were used. These data also represent evidence of small changes in stability with the increasing of the system size, in agreement with HOMA and NO occupation discussed above. The ST splitting present large values in the range of 6.6–6.8 eV, similar to the band gap of the 2D h-BN.<sup>66,67</sup> The  $^3A_1$  state possesses a multiconfigurational character with two dominant configurations related to  $2b_1 \rightarrow 3b_1$  (or  $2b_2 \rightarrow 3b_2$  for borazine) and  $1a_2 \rightarrow 2a_2$  excitations. The orbitals involved in these excitations are very close in energy (see Figures S4–S9 and Figure 5), and therefore, the ST gap may be sensitive to the choice and size of the active space (see below). Once again, this behavior is significantly different from its carbon analogues in which a substantial narrowing of the ST gap is observed as the acene gets bigger, decreasing their stability.<sup>68</sup>

The effects in the selected active space limitation can be observed from the results present in Table 1 in terms of the two energy gaps,  $\Delta E_{1ST}$  and  $\Delta E_{2ST}$ . From BN-tetracene, there is the scenario where not all  $\pi$  electrons are included so there is a difference between  $\Delta E_{1ST}$  and  $\Delta E_{2ST}$ , since the latter one is related to a larger selected active space, therefore, the  $\Delta E_{2ST}$  energies for the largest BN-*n*-acenes calculated give a lower excitation energy, showing that the complete  $\pi$  correlation was more important to the triplet state.

### 3.5 | Excited states of the BN-*n*-acenes

For borazine, all calculations for the lowest singlet excited states indicate the same energetic sequence also observed experimentally<sup>12–14</sup>:  $1^1B_1(1^1A'_2) < 2^1A_1(1^1A'_1) < 2^1B_1$  and  $3^1A_1(1^1E')$ . The state symmetry is given for  $D_{3h}$  (in parentheses) and the actually used in  $C_{2v}$  symmetry. Results obtained at CASSCF and different CASPT2 levels using a

**TABLE 2** Excitation energies (eV) for low-lying states of borazine

Method	$1^1B_1$ ( $1^1A_2$ )	$2^1A_1$ ( $1^1A_1$ )	$2^1B_1/3^1A_1$ ( $1^1E$ )	$1^3A_1$ ( $3^1A_1$ )	$1^3B_1/2^3A_1$ ( $3^1E$ )	$2^3B_1$ ( $3^1A_2$ )
CAS (6,6)–6-31G*						
CASSCF	6.76 [0.000]	8.15 [0.001]	9.03 [0.656]	6.48	7.02	7.81
ic-MRCI + Q – 1s2s	6.93	8.02	8.58	6.82	7.09	7.45
ic-MRCI + Q – 1s	6.83 [0.009]	7.93 [0.001]	8.50 [0.446]	6.71	7.02	7.38
CASPT2 – 1s2s	6.80	7.78	8.30	6.74	6.95	7.21
CASPT2 – 1s	6.56	7.41	7.90	6.57	6.72	6.88
CAS (6,6) – def2-TZVP						
CASSCF	6.66 [0.000]	7.99 [0.006]	8.73 [0.648]	6.39	6.88	7.58
ic-MRCI + Q – 1s2s	6.83	7.84	8.26	6.76	6.96	7.21
ic-MRCI + Q – 1s	6.79 [0.000]	7.82 [0.005]	8.26 [0.509]	6.73	6.96	7.21
CASPT2 – 1s2s	6.62	7.49	7.81	6.60	6.72	6.89
CASPT2 -1 s	6.41	7.15	7.43	6.46	6.51	6.57
Exp.	6.5 <sup>a</sup>	6.56 <sup>b</sup>	7.2 <sup>a</sup> 7.55 <sup>b</sup>			
	6.28 <sup>b</sup>	6.5 <sup>c</sup>	7.5 <sup>c</sup>			
	6.5 <sup>d</sup>	6.7 <sup>d</sup>	7.2 <sup>d</sup>			

Note: Oscillator strengths are given in brackets.

<sup>a</sup>In *n*-heptane solution.<sup>12</sup>

<sup>b</sup>Vapor-phase and matrix-isolated.<sup>14</sup>

<sup>c</sup>Gas phase.<sup>69</sup>

<sup>d</sup>In *n*-heptane solution.<sup>13</sup>

CAS (6,6) are collected in Table 2. The change from 6-31G\* to def2-TZVP leads to a decrease in the excitation energy for all states; this effect is more pronounced for states with higher energy. In comparison with the experimental results, the CASSCF energies for the states  $2^1A_1$  and  $2^1B_1$  are significantly overestimated, requiring the inclusion of dynamic correlation effects to provide more accurate values, as expected.

The ic-MRCI method with Davidson's correction (ic-MRCI + Q) increases the excitation energy for the  $1^1B_1$  state somewhat in comparison to the CASSCF results, while decreasing it for the other singlet states. Comparing with the experimental data,<sup>12–14,69</sup> the ic-MRCI+Q excitation energies computed with both basis sets and with the two schemes of sigma orbital correlation (1s2s and 1s) are overestimated with differences in the range of 0.71–1.52 eV for the states  $2^1A_1$  and  $2^1B_1$ . For the first excited state,  $1^1B_1$ , the ic-MRCI + Q the difference decreases, being larger than the experimental values by 0.29–0.65 eV. In general, the results obtained with CASPT2 present lower excitation energies than those obtained with ic-MRCI + Q, and the correlation of the 2s sigma orbital is more important in the CASPT2, decreasing the excitation energies between 0.14 and 0.40 eV, depending on the excitation and the basis set. Compared to the experimental data, the best results were obtained with CASPT2 (6,6) (1s)/def2-TZVP.

The oscillator strengths, obtained with ic-MRCI/def2-TZVP, correlate well with the experimental assignments, in which the most intense transition is the one to  $2^1B_1$  and  $3^1A_1$  ( $1^1E$ ), with calculated oscillator strength equal to 0.509. For the  $2^1A_1$  ( $1^1A_1$ ) and  $1^1B_1$  ( $1^1A_2$ ) transitions, the oscillator strength is very small, equaling to 0.005 and 0.000, respectively, which explains the low intensity and the difficulty

to be observed experimentally<sup>12–14,69</sup>; additionally, the  $1^1B_1$  ( $1^1A_2$ ) transition is symmetry forbidden.

We have also characterized the three lowest triplet states,  $1^3A_1$  ( $3^1A_1$ ),  $1^3B_1$  and  $2^3A_1$  ( $3^1E$ ), and  $2^3B_1$  ( $3^1A_2$ ) (Table 2). The CASSCF and ic-MRCI show the ( $1^3A_1$  ( $3^1A_1$ )) state as the lowest triplet state. With CASSCF, the increase in the basis set led to a maximum difference of 0.23 eV for  $2^3B_1$  ( $3^1A_2$ ) state with respect to experiment; with ic-MRCI a difference of 0.24 eV. The CASPT2-1s present the  $1^3B_1$  ( $3^1E$ ), and  $2^3B_1$  ( $3^1A_2$ ) states with almost the same energy. Except from CASPT2-1s results, the first triplet state is lower in energy than the first excited singlet for all calculations.

All calculations indicate that the ground state  $X(1^1A_1)$  ( $1^1A_1$ ) is well described by the closed shell HF configuration. With the 6-31G\* basis, the HF configuration contribution is 95% and 81% to the wave function within CASSCF and ic-MRCI methods, respectively. With CASSCF/6-31G\* (Table S10), the first excited singlet state ( $1^1B_1$ ) is described basically by two configurations, related to the excitations  $1a_2 \rightarrow 3b_2$  (44%) and  $2b_2 \rightarrow 2a_2$  (44%). In  $D_{3h}$  symmetry, this state corresponds to the two-electron excitation from HOMO ( $1e''$ )  $\rightarrow$  LUMO ( $2e''$ ). The inclusion of the dynamic correlation with ic-MRCI+Q -1s/6-31G\* indicates that these two configurations contribute with 38%. The second excited singlet state ( $2^1A_1$  ( $1^1A_1$ )) is essentially described by two configurations, related to single excitations  $1a_2 \rightarrow 2a_2$  (HOMO – 1  $\rightarrow$  LUMO) and  $2b_2 \rightarrow 3b_2$  (HOMO  $\rightarrow$  LUMO + 1). The states  $2^1B_1$  and  $3^1A_1$  ( $1^1E$ ) possess a characterization similar to the  $1^1B_1$  ( $1^1A_2$ ) state.

The most stable triplet state  $1^3A_1$  ( $3^1A_1$ ) has two dominant configurations,  $1b_2^2 2b_2^1 3b_2^1 4b_2^0 1a_2^2 2a_2^0$  and  $1b_2^2 2b_2^2 3b_2^0 4b_2^0 1a_2^1 2a_2^1$ , with similar contributions, equal to 43% and 37% at CASSCF and

ic-MRCI + Q – 1s/6-31G\*, respectively. The  $1^3B_1$  ( $^3A'_2$ ) and  $2^3B_1$  ( $^3A'_2$ ) states are predominantly described by the configurations  $1b_2^{-2} 2b_2^{-1} 3b_2^0 4b_2^0 1a_2^{-2} 2a_2^{-1}$  (44%) and  $1b_2^{-2} 2b_2^{-2} 3b_2^{-1} 4b_2^0 1a_2^{-1} 2a_2^0$  (44%) (Table S10).

Due to the aforementioned alternant character of the HOMO and LUMO in terms of contributions of nitrogen and boron atoms, the electronic excitations in the BN-*n*-acenes are connected with a charge transfer. The density difference plots between the ground state and the first excited singlet ( $1^1B_1$ ) state for borazine and BN-pentacene is shown in Figure 7A,B, respectively, indicating the charge transfer from nitrogen to boron. In the case of the BN-pentacene, the density located in the outer rings are in agreement with the orbitals involved in the excitations, see Figure 5, this behavior also happens for the larger systems in the series of the BN-*n*-acenes, Figure S10. The density differences show similar charge transfer from nitrogen to boron for the other excited states as well.

The results obtained for the vertical excitation energies for BN-naphthalene are shown in Table 3. The CASSCF excitation energy for the  $1^1B_2$  state is strongly dependent on the size of the active spaces, ranging from CAS (4,4), CAS (8,8) to the complete valence  $\pi$  space

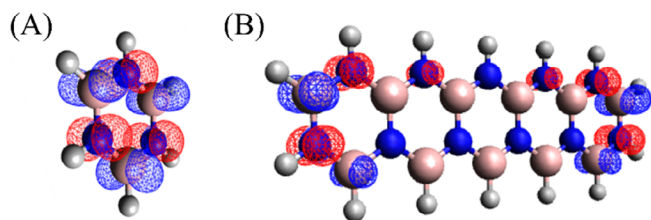


**FIGURE 7** Density difference between the first singlet excited state ( $1^1B_1$ ) and the ground state ( $X^1A_1$ ) for (A) borazine in and (B) for BN-pentacene calculated at CASPT2(6,6)-1s2s/6-31G\* level for borazine and CASPT2(8,7)-1s2s/6-31G\* for BN-pentacene. Blue regions indicate positive sign (density gain) and red indicates negative sign (density loss); isovalue is  $0.004 \text{ e}/\text{\AA}^3$

(10,10). A similar sensitivity toward the size of the active space was observed also for the same state in naphthalene.<sup>48</sup> Considering the CASSCF (10,10), the  $1^1B_2$  state is characterized by two dominant configurations resulting from single excitations,  $3b_1$  (HOMO – 1)  $\rightarrow$   $3a_2$  (LUMO) (36%) and  $2a_2 \rightarrow$  (HOMO)  $\rightarrow$   $4b_1$  (LUMO + 1) (36%), which are similar to the same state of naphthalene.<sup>48</sup> The inclusion of dynamic correlation with the CASPT2 method, in general, reduces significantly the dependence of the excitation energies on the choice of the active space.

The CASSCF excitation energies for the  $2^1A_1$  state present large variation with the size of the active space ((4,4), (8,8) and (10,10)) as well. This state is mainly described by the excitation  $2a_2$  (HOMO)  $\rightarrow$   $3a_2$  (LUMO) (70%). As observed for the  $1^1B_2$  state, the CASPT2 energies present small variation, with the size of the active space for both (1s) and (1s2s) freezing scheme. The excitation energy for  $2^1B_2$  state is about 1 eV higher than the  $2^1A_1$  state with CASSCF, decreasing to about 0.7 eV with CASPT2.

The values for the oscillator strength indicate that the transition to the  $2^1B_2$  state dominates the ones to the other singlet states. The energetic order of the singlets excited states obtained with our best computational settings, CASPT2 (10,10) (1s), are  $2^1B_2$ ,  $2^1A_1$ , and  $2^1B_2$ .

The  $1^3A_1$  triplet state has a dominant configuration with  $2a_2$  and  $3a_2$  unpaired orbitals (72%). The excitation energy is dependent on the size of the active space but with a much smaller dependence related to the correlation of the 2s sigma orbitals. Our best results calculated with CASPT2 (10,10) (1s) characterizes the triplet  $1^3A_1$  state as the first excited triplet state, located 6.42 eV above the ground state, which is only 0.21 eV above the first singlet  $1^1B_2$  excited state.

For BN-anthracene, the results calculated for the vertical excitation energies are presented in Table 4. The first singlet excited state,  $1^1B_2$ , has a multiconfigurational character, with two dominant configurations similar to that observed in BN-naphthalene. The  $2^1A_1$  state is close in energy to the  $1^1B_2$  state.

Method	$1^1B_2$	$2^1A_1$	$2^1B_2$	$1^3A_1^a$
CAS (4,4)				
CASSCF	8.55	9.09	9.50	7.28
CASPT2 – 1s2s	6.72	7.11	7.32	6.87
CASPT2 – 1s	6.21	6.54	6.72	6.80
CAS (8,8)				
CASSCF	7.22 [0.250]	8.19 [0.431]	9.06 [0.726]	7.21
CASPT2 – 1s2s	6.59	7.01	7.60	6.69
CASPT2 – 1s	6.23	6.56	7.09	6.61
CAS (10,10)				
CASSCF	6.80 [0.014]	7.47 [0.229]	8.41 [1.079]	6.65
CASPT2 – 1s2s	6.52	6.92	7.67	6.59
CASPT2 – 1s	6.21	6.53	7.24	6.42

Note: Oscillator strength values in brackets.

<sup>a</sup>Calculated using state averaged with fourth triplet states (two  $A_1$  and two  $B_2$ ).

**TABLE 3** Excitation energies (eV) for low-lying states of BN-naphthalene calculated with 6-31G\* basis set

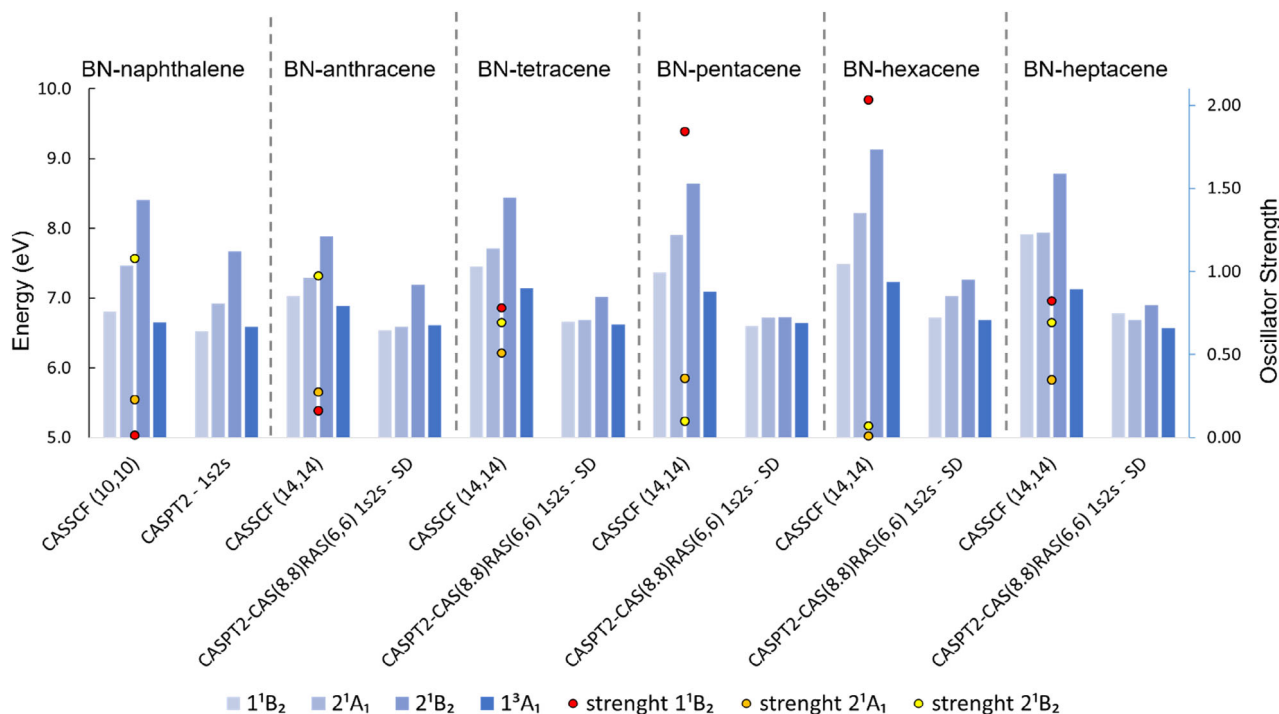


**TABLE 4** Excitation energies (eV) for low-lying states of BN-anthracene calculated with 6-31G\* basis set

Method	$1^1B_2$	$2^1A_1$	$2^1B_2$	$1^3A_1^a$
CAS (8,8)				
CASSCF	7.86 [1.087]	8.66 [0.200]	9.44 [0.005]	7.35
CASPT2 – 1s	6.42	6.25	6.75	6.65
CASPT2 – 1s2s	6.86	6.83	7.40	6.76
CAS (14,14)				
CASSCF	7.03 [0.162]	7.29 [0.273]	7.88 [0.973]	6.89
CASPT2 – 1s	6.15	6.16	6.76	6.44
CASPT2 – 1s2s	6.54	6.59	7.19	6.62
CASPT2-CAS(8,8)RAS (6,6)-SD – 1s2s	6.54	6.59	7.19	6.61

Note: Oscillator strength values in brackets.

<sup>a</sup>Calculated using state averaged with fourth triplet states (two  $A_1$  and two  $B_2$ ).

**FIGURE 8** Excitation energies (eV) for low-lying states of BN-*n*-acyenes and oscillator strengths calculated with the 6-31G\* basis set

The oscillator strength values obtained from the CASSCF (14,14) calculation indicate that, in the same way as in BN-naphthalene, the transition to  $2^1B_2$  state is much more intense ( $f = 0.973$ ) than the transitions to  $1^1B_2$  ( $f = 0.162$ ) and  $2^1A_1$  ( $f = 0.273$ ) states.

Also, it is important to highlight the comparison between the results from the combination of the CAS (8,8) + RAS (6,6) approach with the ones obtained with the full  $\pi$  space CAS (14,14). As one can note, they are equivalent, and therefore the former space will be used as a cost-effective choice for the calculation of the larger BN systems.

For the larger systems, BN-tetracene to BN-heptacene, we have used the aforementioned CAS + RAS combination, CAS (8,8)RAS (6) (SD). The results for the vertical low-lying singlet excitation energies are presented in Figure 8 (see Table S11 for the numerical values of these energies). For all systems, as observed for BN-naphthalene and BN-anthracene, the three low-lying singlet states are close in

energy, and they are related to the excitations of the frontier HOMOs orbitals which present the densities mostly on the nitrogen atoms to the LUMOs orbitals mostly on the boron atoms (Figures S4–S9 and Figure 5). The energies of the first singlet excited states are lower than 6.8 eV at CASPT2 level, without significant changes as the system's size increase. Figure 8 also illustrates the almost constant trend of the singlet-triplet splitting, as the darker blue column, as discussed before, with CASPT2 values around of 6.6 eV.

## 4 | CONCLUSIONS

The electronic structure, bonding in the ground state and the UV spectra of BN-*n*-acyenes have been investigated by means of high-level single reference and multireference methods. Since the boron

and nitrogen atoms form an isoelectronic pair of two carbon atoms, the BN-*n*-acenes have been considered as a complete substitution of the BN units into molecules of the acene series. The obtained substitution products exhibit substantially elevated stability in comparison to the acenes. The structural analysis explains the observed effects as originating from the insertion of a uniform pattern of electronegativity difference into the acene series. The covalent bonds tend to be strongly polarized which does not occur in the case of a carbon-only framework. This leads to a charge transfer between neighboring atoms resulting in more stabilized structures as shown by the population analysis. Due to the unoccupied  $\pi$  orbital in the boron atom, it attracts density from nitrogen in the  $\pi$  domain but donates  $\sigma$  density to nitrogen because of electronegativity differences. The total boron net charge in the BN-*n*-acenes is positive. This charge transfer mechanism also shows that the resulting charge is dependent on the connectivity of the atoms. Boron atoms connected to three nitrogens have a more positive net charge than those connected only to two nitrogen atoms. Due to the rigid charge structure, there are no significant changes in properties as the system grows. For example, the aromaticity remains almost constant when measured by HOMA values. The singlet-triplet splitting also agrees with this stability trend, maintaining a consistent gap value for the molecules. The electronic excitations are always connected with charge transfer since in the HOMO nitrogen atoms are populated whereas in the LUMO the population is located on the boron atoms.

The coexistence of boron and nitrogen atoms results in  $\pi$  molecular orbitals spatially localized, which reduces the spatial overlap and therefore the influence on the energy splitting of the orbitals as the system grows. This indicates electronic properties that show small variations with the increase in system size, a feature strikingly different from its carbon counterpart. This is supported by the results, in which bond lengths, S-T energy separation, excitation energies and natural orbital occupations essentially do not have a strong dependence on the number of BN rings and these systems present a relatively high stability. Electronic devices based on (carbon) *n*-acenes would involve a control of its size to satisfy the required properties for a given device, since one extra ring or one less substantially changes its energetics and stability, in practice limiting the usage of such devices up to pentacene (not considering other approaches to control the acene stability). On the other hand, the properties of the BN-*n*-acenes are mostly known even before defining their size, at least for the range of compounds studied in the present work. Both the size dependence/independence behavior of carbon/BN acenes have advantages and disadvantages and it could be expected that they can probably complement each other when using these materials as building blocks in nanoengineering and nanoelectronics in future molecular electronic devices.

## ACKNOWLEDGMENTS

This work has been supported by Brazilian agencies Fundação de Amparo à Pesquisa do Estado de São Paulo (FAPESP) under grants 2019/25105-6, and 2019/03729-8, and Conselho Nacional de Desenvolvimento Científico e Tecnológico (CNPq) under grants

307136/2019-1 and 313624/2019-4. This material is based also upon work supported by the National Science Foundation under Grant No. 2107923.

## DATA AVAILABILITY STATEMENT

The data that support the findings of this study are available from the corresponding author upon reasonable request.

## ORCID

Francisco B. C. Machado  <https://orcid.org/0000-0002-2064-3463>

## REFERENCES

- [1] R. Islas, E. Chamorro, J. Robles, T. Heine, J. C. Santos, G. Merino, *Struct. Chem.* **2007**, *18*, 833.
- [2] A. Kumar, S. Sarvesh, K. Pandey, N. Misra, *Theor. Chem. Accounts* **2016**, *135*(158), 1.
- [3] H. Jacobsen, *Chem. Phys. Lett.* **2013**, *582*, 144.
- [4] B. Kiran, A. K. Phukan, E. D. Jemmis, *Inorg. Chem.* **2001**, *40*, 3615.
- [5] A. K. Phukan, R. P. Kalagi, S. R. Gadre, E. D. Jemmis, *Inorg. Chem.* **2004**, *43*, 5824.
- [6] O. R. Lourie, C. R. Jones, B. M. Bartlett, P. C. Gibbons, R. S. Ruoff, W. E. Buhro, *Chem. Mater.* **2000**, *12*, 1808.
- [7] R. T. Paine, L. G. Sneddon, *Chemtech* **1994**, *7*, 29.
- [8] J. Eichler, C. Lesniak, *J. Eur. Ceram. Soc.* **2008**, *28*, 1105.
- [9] Q. Weng, X. Wang, C. Zhi, Y. Bando, D. Golberg, *ACS Nano* **2013**, *7*(2), 1558.
- [10] P. G. Campbell, L. N. Zakharov, D. J. Grant, D. A. Dixon, S. Y. Liu, *J. Am. Chem. Soc.* **2010**, *132*, 3289.
- [11] J. R. Platt, H. B. Kleven, G. W. Schaeffer, *J. Chem. Phys.* **1947**, *15*, 598.
- [12] L. E. Jacobs, J. R. Platt, G. W. Schaeffer, *J. Chem. Phys.* **1948**, *16*, 116.
- [13] C. W. Rector, G. W. Schaeffer, J. R. Platt, *J. Chem. Phys.* **1949**, *17*, 460.
- [14] A. Kaldor, *J. Chem. Phys.* **1971**, *55*, 4641.
- [15] C. C. J. Roothaan, R. S. Mulliken, *J. Chem. Phys.* **1948**, *16*, 118.
- [16] M. Davies, G. H. Thomas, *Trans. Faraday Soc.* **1960**, *56*, 185.
- [17] O. Chalvet, R. Dandel, J. J. Kaufman, *J. Am. Chem. Soc.* **1965**, *87*, 399.
- [18] W. F. Young, F. Grein, J. Passmore, I. Unger, *Can. J. Chem.* **1971**, *49*, 233.
- [19] M. A. Hague, A. B. Sannigrahi, B. G. Niyogi, *J. Phys. Chem.* **1979**, *83*, 1348.
- [20] P. M. Kuznesof, D. F. Shriver, *J. Am. Chem. Soc.* **1968**, *90*, 1683.
- [21] S. D. Peyerimhoff, *Theor. Chim. Acta* **1970**, *19*, 1.
- [22] V. Deshmukh, M. Nagnathappa, B. Kharat, A. Chaudhari, *J. Mol. Liq.* **2014**, *193*, 13.
- [23] A. W. Laubengayer, P. C. Moews, R. F. Porter, *J. Am. Chem. Soc.* **1961**, *83*, 1337.
- [24] G. Manatov, J. L. Margrave, *J. Inorg. Nucl. Chem.* **1961**, *20*, 348.
- [25] P. J. Fazen, E. E. Remsen, J. S. Beck, P. J. Carroll, A. R. Mcghee, G. S. Larry, *Chem. Mater.* **1995**, *7*, 1942.
- [26] T. Kar, D. E. Elmore, S. J. Scheiner, *Mol. Struct.* **1997**, *392*, 65.
- [27] A. S. Lisovenko, A. Y. Timoshkin, *Russ. Chem. Bull.* **2015**, *64*, 2573.
- [28] T. Kato, T. Yamabe, *New J. Chem.* **2003**, *118*, 3804.
- [29] A. J. L. Catão, A. López-Castillo, *J. Mol. Model.* **2017**, *23*(119), 1.
- [30] P. K. Chattaraj, D. R. Roy, *J. Phys. Chem. A* **2007**, *111*, 4684.
- [31] C. Möller, M. S. Plasset, *Phys. Rev.* **1934**, *46*, 618.
- [32] F. Weigend, R. Ahlrichs, *Phys. Chem. Chem. Phys.* **2005**, *7*, 3297.
- [33] T. M. Krygowski, *J. Chem. Inf. Comput. Sci.* **1993**, *33*, 70.
- [34] I. D. Madura, T. M. Krygowski, M. K. Cyrański, *Tetrahedron* **1998**, *54*, 14913.
- [35] P. G. Szalay, R. J. Bartlett, *Chem. Phys. Lett.* **1993**, *214*, 481.
- [36] B. O. Roos, P. R. Taylor, *Chem. Phys.* **1980**, *48*, 157.

- [37] P. Siegbahn, A. Heiberg, B. O. Roos, *Phys. Scr.* **1980**, 21, 323.
- [38] P. Siegbahn, J. Almlöf, A. Heiberg, B. O. Roos, *J. Chem. Phys.* **1981**, 74, 2384.
- [39] P. J. Knowles, H. Werner, *Chem. Phys. Lett.* **1988**, 145, 514.
- [40] K. R. Shamasundar, G. Knizia, H. Werner, *J. Chem. Phys.* **2011**, 135(54101), 1.
- [41] H. Werner, P. J. Knowles, *J. Chem. Phys.* **1988**, 89, 5803.
- [42] S. R. Langhoff, E. R. Davidson, *Int. J. Quantum Chem.* **1974**, 8, 61.
- [43] D. C. Rawlings, E. R. Davidson, M. Gouterman, *Int. J. Quantum Chem.* **1984**, 26, 251.
- [44] R. Ditchfield, W. J. Hehre, J. A. Pople, *J. Chem. Phys.* **1971**, 54, 724.
- [45] A. Bunge, *J. Chem. Phys.* **1970**, 53, 20.
- [46] P. Celani, H. J. Werner, *J. Chem. Phys.* **2000**, 112, 5546.
- [47] H. Werner, *Mol. Phys.* **1996**, 89, 645.
- [48] F. Bettanin, L. F. A. Ferrão, M. Pinheiro, A. J. A. Aquino, H. Lischka, F. B. C. Machado, D. Nachtigallova, *J. Chem. Theory Comput.* **2017**, 13, 4297.
- [49] M. J. Frisch, *Gaussian 9 Revision B*, Gaussian Inc., Wallingford **2016**.
- [50] H. Werner, P. J. Knowles, G. Knizia, F. R. Manby, M. Schutz, *WIREs Comput. Mol. Sci.* **2012**, 2, 242.
- [51] H. Lischka, R. Shepard, T. Müller, P. G. Szalay, R. M. Pitzer, A. J. A. Aquino, M. M. A. Nascimento, M. Barbatti, L. T. Belcher, J. P. Blaudeau, I. Borges Jr., S. R. Brozell, E. A. Carter, A. Das, G. Gidofalvi, L. Gonzalez, W. L. Hase, G. Kedziora, M. Kertesz, F. Kossoski, F. B. C. Machado, S. Matsika, S. A. Monte, D. Nachtigallova, R. Nieman, M. Oppel, C. A. Parish, F. Plasser, R. F. K. Spada, E. A. Stahlberg, E. Ventura, D. R. Yarkony, Z. Zhang, *J. Chem. Phys.* **2020**, 152(134110), 1.
- [52] H. Lischka, T. Müller, P. Szalay, I. Shavitt, R. Pitzer, R. Shepard, *WIREs Comput. Mol. Sci.* **2011**, 1, 191.
- [53] M. Pinheiro, L. F. A. Ferrão, F. Bettanin, A. J. A. Aquino, F. B. C. Machado, H. Lischka, *Phys. Chem. Chem. Phys.* **2017**, 19, 19225.
- [54] J. Poater, J. M. Bofill, P. Alemany, M. Sola, *J. Phys. Chem. A* **2005**, 109, 10629.
- [55] P. Bultinck, M. Rafat, R. Ponc, B. Van Gheluwe, R. Carbo-Dorca, P. Popelier, *J. Phys. Chem. A* **2006**, 110, 7642.
- [56] T. Ishida, J. Aihara, *Phys. Chem. Chem. Phys.* **2009**, 11, 7197.
- [57] D. Setiawan, E. Kraka, D. Cremer, *J. Org. Chem.* **2016**, 81, 9669.
- [58] M. Pinheiro, A. Das, A. J. A. Aquino, H. Lischka, F. B. C. Machado, *J. Phys. Chem. A* **2018**, 122, 9464.
- [59] B. D. Milanez, J. C. V. Chagas, M. Pinheiro, A. J. A. Aquino, H. Lischka, F. B. C. Machado, *Theor. Chem. Accounts* **2020**, 139(113), 1.
- [60] M. Pinheiro, F. B. C. Machado, F. Plasser, A. J. A. Aquino, H. Lischka, *J. Mater. Chem. C* **2020**, 8, 7793.
- [61] S. Manzetti, T. Lu, *J. Phys. Org. Chem.* **2013**, 26, 473.
- [62] T. Lu, S. Manzetti, *Struct. Chem.* **2014**, 25, 1521.
- [63] F. Plasser, H. Pašalić, M. H. Gerzabek, F. Libisch, R. Reiter, J. Burgdörfer, T. Müller, R. Shepard, H. Lischka, *Angew. Chem. Int. Ed.* **2013**, 52, 2581.
- [64] T. Shimazaki, T. Nakajima, *Phys. Chem. Chem. Phys.* **2016**, 18, 27554.
- [65] Y. Yang, E. R. Davidson, W. Yang, *Proc. Natl. Acad. Sci.* **2016**, 113, E5098.
- [66] A. Nagashima, N. Tejima, Y. Gamou, T. Kawai, C. Oshima, *Phys. Rev. B* **1995**, 51, 4606.
- [67] L. H. Li, Y. Chen, *Adv. Funct. Mater.* **2016**, 26, 2594.
- [68] S. Horn, F. Plasser, T. Müller, F. Libisch, J. Burgdörfer, H. Lischka, *Theor. Chem. Accounts* **2014**, 133(1511), 1.
- [69] E. R. Bernstein, J. P. Reilly, *J. Chem. Phys.* **1972**, 57, 3960.

## SUPPORTING INFORMATION

Additional supporting information can be found online in the Supporting Information section at the end of this article.

**How to cite this article:** B. D. Milanez, G. M. dos Santos, M. Pinheiro Jr, L. T. Ueno, L. F. A. Ferrão, A. J. A. Aquino, H. Lischka, F. B. C. Machado, *J. Comput. Chem.* **2023**, 44(6), 755. <https://doi.org/10.1002/jcc.27038>